Bioactive Materials 6 (2021) 2658–2666

Contents lists available at ScienceDirect

Bioactive Materials

journal homepage: www.sciencedirect.com/journal/bioactive-materials

Pro-osteogenesis and *in vivo* tracking investigation of a dental implantation system comprising novel mTi implant and HYH-Fe particles

Xiyu Li [a], Juan Wu [a], Danxue Li [a], Qin Zou [b,*], Yi Man [a], Ling Zou [a], Wei Li [a,**]

[a] State Key Laboratory of Oral Diseases & National Clinical Research Center for Oral Diseases, West China Hospital of Stomatology, Sichuan University, Chengdu, 610041, China
[b] Analytical and Testing Center, Sichuan University, Chengdu, 610064, China

ARTICLE INFO

Keywords:
Pro-osteogenesis
mTi implant
Local static magnetic field
Superparamagnetic particles
In vivo tracking

ABSTRACT

Insufficient early osteogenesis seriously affects the later stage osteogenic quality and osseointegration of dental implants. To promote early osteogenesis, we first designed a Ti dental implant with a built-in magnet (mTi) to produce a local static magnetic field (SMF). Then, a dental implantation system comprising the mTi implant and the superparamagnetic hydroxyapatite (HA:Yb/Ho–Fe, named HYH-Fe) particles was implanted into the alveolar bone of beagles. The results showed that the mTi + HYH-Fe group displayed better early osteogenesis and later stage osseointegration than the Ti + HA and mTi + HA groups. A combination of the local SMF (mTi) and superparamagnetic HYH-Fe particles had a positive effect on the pro-osteogenesis of Ti implants. The results also indicated that week 10 could be adopted as the key time point to evaluate the early osteogenic effect of the mTi + HYH-Fe implantation system, which would be a promising prospect for promotion of osteogenesis, *in vivo* tracking investigation of material-bone relationships, and clinical applications.

1. Introduction

Biomaterials are playing an increasingly important role in promoting the development of regenerative medicine and improving the quality of life [1,2]. There are a large number of patients with tooth loss due to disease, trauma, and aging each year. Although titanium (Ti) dental implants and hydroxyapatite (HA) fillers have been broadly used in tooth loss repair [3,4], insufficient early osteogenesis around the implant is a crucial factor in the loosening or detachment of the implants [5,6]. How to promote early osteogenesis and improve the osseointegration is still a clinical challenge to be addressed.

In clinic, the new bone tissue usually takes approximately 3 months to form a stable osseointegration with implants [7,8]. It is necessary to accelerate the growth of new bone around the Ti implants and improve the osseointegration between Ti implants and new bone tissue. To accelerate the osseointegration, titanium implants are usually undergone surface modification such as sand blasting, acid etching, and chemical modification to get a rough and hydrophilic surface for bone contact [9,10]. The osteogenesis of HA material is mainly reflected in the formation of bone-bonding with new bone tissues [4,11], yet its effect on promoting early osteogenesis is not strong enough. Therefore, the strategy of promoting early bone formation with the help of growth factors (such as bone morphogenetic protein-2, BMP-2) has been widely adopted [12,13]. However, despite the pro-osteogenic effect of BMP-2, its clinical use has shown a risk of heterotopic bone formation or complications of postoperative inflammatory swelling, etc. [14,15]. Recently, immune regulation of early inflammatory cells has been used to regulate the recruitment and osteogenic differentiation of stem cells [15,16], but its promoting effect on early osteogenesis *in vivo* remains unknown and needs further investigation. So far, researchers are still searching for effective methods to promote early bone formation and to improve the osseointegration.

The use of magnetic fields to promote early osteogenesis may be an effective, low-cost, and low-risk approach, particularly when using a static magnetic field (SMF). Some previous studies have shown that a moderate-intensity SMF (mT level) can facilitate cell proliferation, neovascularization processes, and bone healing [17–19]. Both *in vitro* cell cultures and *in vivo* experiments in mice or rabbits have demonstrated that SMF could be an effective treatment tool for bone fractures and defects [20–23]. However, there is a lack of investigation into early

Peer review under responsibility of KeAi Communications Co., Ltd.
* Corresponding author.
** Corresponding author.
E-mail addresses: zouqin80913@126.com (Q. Zou), leewei@scu.edu.cn (W. Li).

https://doi.org/10.1016/j.bioactmat.2021.01.038
Received 17 November 2020; Received in revised form 19 January 2021; Accepted 30 January 2021
Available online 12 February 2021

osteogenesis of SMF and on a combination of SMF and superparamagnetic HA particles in the oral environment of large animals, which are important for future clinical applications in improving the repair effect of dental implants. For this reason, we selected beagle dogs to carry out the oral implantation experiment.

In the study, we designed a Ti implant with built-in magnet (mTi) to provide the local SMF, and prepared a superparamagnetic/upconversion fluorescent HA:Yb/Ho–Fe (HYH–Fe) particles, which were together implanted into the alveolar bone of beagle dogs. The effect of SMF and superparamagnetic HA particles on early osteogenesis was examined by micro-CT reconstruction, histological analysis, and confocal fluorescent imaging, as well as by the in situ sequential fluorescent labeling of new bone tissue. Three fluorochromes, calcein, alizarin red, and tetracycline were employed for the sequential fluorescent labeling at three different time points, to trace the regeneration and reconstruction process of new bone tissue at different implantation stages [24,25]. These fluorochromes have an ability to chelate with calcium ions to form complexes that deposit into bone tissue during bone formation [26]. In addition, the doping of Yb and Ho ions in HA matrix also endows an upconversion fluorescence due to the energy transfer of Yb to Ho ions [27] and CT tracking capacities due to the high X-ray absorbability of Yb ions [28], which is beneficial to distinguish the implanted HA particles during osteogenesis, including their distribution in bone tissue and interrelation with bone tissues.

Meanwhile, Ti implants with or without built-in magnets together with pure HA particles were employed as the control groups (i.e., mTi + HA group and Ti + HA group) to investigate comparatively with the mTi + HYH-Fe group. The research mainly focused on the early osteogenesis during a period of 8–12 weeks (2–3 months). The in situ sequential fluorescent labeling was performed via intramuscular injection of calcein at 8 weeks, alizarin red at 10 weeks, and tetracycline at 12 weeks. Tracking of the early formation process and growth trend of the new bone tissue would reveal the osteogenic promotion effect of the mTi implant and superparamagnetic HYH-Fe combination, laying a foundation for future clinical applications.

2. Materials and methods

2.1. Reagents

Analytical grade $Ca(NO_3)_2{\cdot}4H_2O$, $Na_3PO_4{\cdot}12H_2O$, and $Fe(NO_3)_3$ were obtained from Kelong Chemical Reagent Co. Ltd. (Chengdu, China). Analytical grade $Yb(NO_3)_3{\cdot}6H_2O$ and $Ho(NO_3)_3{\cdot}6H_2O$ were purchased from Aladdin Reagents (Shanghai, China). Other chemical reagents were used without further purification.

2.2. Preparation of upconversion HYH particles

The Yb^{3+} and Ho^{3+} ions were doped into hydroxyapatite to prepare the HYH particles. Briefly, an aqueous solution of Na_3PO_4 (0.20 M, 7 mL) was slowly added to a solution containing $Ca(NO_3)_2$ (0.28 M, 7 mL), $Yb(NO_3)_3$ (0.10 M, 2 mL), and $Ho(NO_3)_3$ (0.01 M, 2 mL) under magnetic stirring in a Teflon autoclave (50 mL). The reaction formula was as follows, $8.9Ca(NO_3)_2 + 1.0\ Yb(NO_3)_3 + 0.1Ho(NO_3)_3 + 6Na_3PO_4 \rightarrow (Ca_{8.9}Yb_1Ho_{0.1})(PO_4)_6(OH)_2$, and the molar ratio of the Ca^{2+}, Yb^{3+}, and Ho^{3+} ions was set to 8.9/1/0.1. The mixture was then hydrothermally treated at 120 °C for 10 h. After cooled to room temperature, the resulting precipitate was collected by centrifugation (10 min at 2700×*g*) and rinsed three times in deionized (DI) water. After freeze-drying, the HYH powder was activated in a muffle furnace (KSL-1200X-J, Kejing, China), at 700 °C for 2 h at a heating rate of 1 °C/min to induce upconversion fluorescence and solidified the crystal structure [27]. For comparison, pure HA powder was also prepared without the doping of Yb^{3+} and Ho^{3+} ions and sintered at 700 °C for 2 h.

2.3. Preparation of superparamagnetic/upconversion HYH-Fe particles

The ion exchange hydrothermal method was employed similar to the previous work [7]. The HYH particles (0.5 g in 20 mL of DI water) were mixed in $Fe(NO_3)_3$ solution (0.5 g, 20 mL), and hydrothermally treated at 160 °C for 6 h to facilitate Fe^{3+} ions to exchange Ca^{2+} ions on the surface region of the HYH particles. The HYH-Fe product was collected by centrifugation, fully washed with DI water, and freeze-dried.

2.4. Design and fabrication of mTi implants

Commercially available medical grade pure titanium (Ti) rods of 5.0 mm in diameter (TA1, Baoji Titanium Industry Co., Ltd., China) were used to machine the Ti dental implants (ϕ 3.0 × 7.0 mm) with inner extended channel (ϕ 1.2 × 3.0 mm) and external thread. The surface of the Ti dental implants were sand blasted, mixed-acid etched in 63.6 wt% H_2SO_4 for 1 h and 10.6 wt% HCl for 1 h and treated with alkali (5 mol/L NaOH) for 1 h. The inner extended channel in Ti implant was designed for placing small magnet to produce a moderate local static magnetic field (SMF). That is, a neodymium small magnet (NdFeB, N35, ϕ 1.0 × 2.0 mm, Qingdao Qiangsheng Magnets Co., China) was selected to insert into the Ti implant, which was then sealed by a titanium sealing screw (Fig. 1).

2.5. Characterization

Transmission electron microscopy (TEM) image and selected area electron diffraction (SAED) pattern were acquired by a FEI TecnaiG2 T20 instrument (USA) at 200 kV. X-ray powder diffraction (XRD) patterns were collected using a PANalytical Empyrean instrument (The Netherlands) over a 2θ range from 20° to 60° in the presence of Cu Kα radiation (λ = 1.5406 Å). The Fourier transform infrared (FTIR) spectra were recorded by Nicolet 6700 (Thermo Fisher Scientific, USA) in the transmission mode with a wavenumber range of 500–4000 cm^{-1}. The elements and binding energy were measured using X-ray photoelectron spectroscopy (XPS) with an AXIS Ultra DLD instrument (Kratos, UK). The magnetic intensities of the magnet and the Ti implant with a built-in magnet (mTi) were measured using a Gaussmeter (HT20, Hengtong, China). The room temperature magnetization curve was recorded using a vibrating sample magnetometer (VSM, Lakeshore 7410, USA). The harvested animal samples were scanned using microcomputed tomography (micro-CT, Viva CT80, SCANCO Medical AG, Switzerland) and observed using a laser scanning confocal microscope (LSCM, Nikon A1R MP+, Japan).

2.6. Cell culture and proliferation

The osteoblastic MG63 cells were cultured in F12 medium (GIBCO, USA) supplemented with 10% fraction of calf serum (GIBCO, USA) and 1% penicillin and streptomycin (100 U/ml, GIBCO, USA), and maintained in a humidified incubator (37 °C, 5% CO_2). The medium was replaced every two days, and regular subculturing was carried out with 0.25% trypsin. Then, MG63 cells were cultured with HA or HYH-Fe solution (100 μg/mL) under the presence of SMF by attaching magnets on the back of culture plates. The cells were seeded into 96-well tissue culture plates (Corning, USA) at a density of 2×10^4 cells/well. The seeded samples were cultured at 37 °C, with 5% CO_2 and 90% humidity, and the medium was changed every two days. MG63 cells cultured in F12 medium with or without SMF served as the control. After incubation for 1, 4, and 7 days, samples were evaluated using a CCK-8 assay, and the optical density (OD) value of the solution was recorded using a microplate reader (PerkinElmer Wallac 1420) at 490 nm to determine cell proliferation.

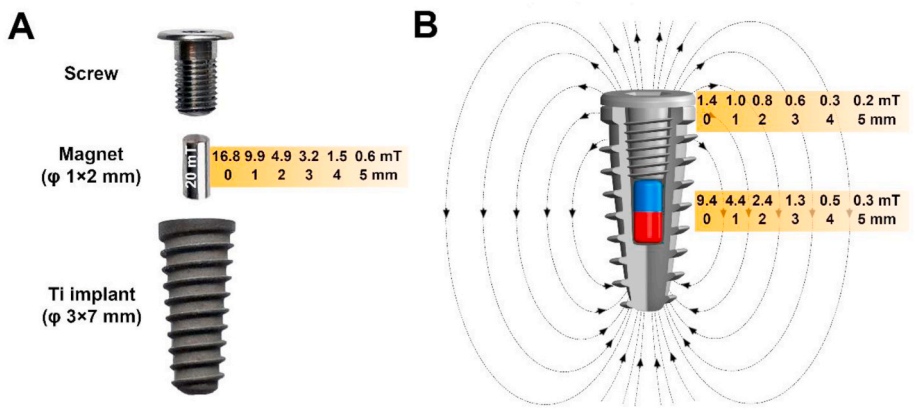

Fig. 1. The assembly structure and the static magnetic field (SMF) intensity distribution. The assembly structure (A) and the magnetic intensity distribution (B) of the mTi implant.

2.7. Animal experiments

The animal experiments were performed according to protocols approved by the Research Ethics Committee of the State Key Laboratory of Oral Diseases, West China Hospital of Stomatology, Sichuan University with an authorization number of WCHSIRB-D-2016-134. Two inbred beagle dogs (male, ~10 kg) around 18 months old were used in this study. All surgical procedures were administered under generalized anesthesia induced by ketamine/xylazine (1 mL/kg) and kept in a sterile operating room, and the beagle dogs were taken for local anesthesia using lidocaine (20 mg/kg). The right and left mandibular second, third, and fourth premolars (PM2, PM3, PM4) were extracted using dental forceps, the mesial roots and distal roots were extracted atraumatically, during which all buccal bone walls were kept intact and granulation tissue was removed completely. Then a guide drill and tapping drills of 2 mm, 2.8 mm and finally 3 mm were used to drill the mesial root socket to obtain an implantation site of totally 8 mm in depth. The Ti and mTi implants, as well as HA and HYH-Fe powders were randomly divided into three groups (n = 2): Ti + HA group, mTi + HA group, and mTi + HYH-Fe group (Fig. S1A). The mTi implant was inserted in the implantation site of mesial root using a torque wrench (Fig. S1B) and the superparamagnetic HYH-Fe particles were filled in the bone cavity surrounding the implant. Meanwhile, Ti + HA group and mTi + HA group were implanted similarly. The distal roots were filled with the Bio-Oss powder to prevent possible bone resorption and effect to the implant after implantation. Afterwards, tension-reduced suture was performed, and no exposure of implants and powder materials was detected.

The 12-week implantation groups were administered for the in situ sequential fluorescence labeling during the implantation period. Three fluorochromes were injected intramuscularly at a sequence of 25 mg/kg calcein (Sigma–Aldrich) at 8 weeks, 30 mg/kg alizarin red (Sigma–Aldrich) at 10 weeks, and 25 mg/kg tetracycline hydrochloride (Sigma–Aldrich) at 12 weeks. Samples were harvested with surrounding tissue at 8 weeks (dog 1) and 12 weeks (dog 2) after implantation and fixed in 4% buffered paraformaldehyde and scanned and reconstructed by micro-CT. The bone volume fraction (BV/TV), trabecular number (Tb. N), trabecular thickness (Tb. Th) and trabecular separation (Tb. Sp) were measured by SCANCO μCT Evaluation Program. The bones of 1 mm around Ti or mTi implants were reconstructed from CT scan images via image processing. The scanning threshold range was set for 220–500, which could well exclude the image of metal implants and was conducive to the display of new bone tissue as much as possible. After micro-CT reconstruction, the fixed samples were then embedded in polymethyl methacrylate (PMMA) and cut into thin sections after being dehydrated through gradient ethanol and cleaned in xylene, and stained with Stevenel's blue/van Gieson's picrofuchsin to stain calcified bone bright red and soft tissue blue. The sections were then analyzed under a digital microscope (ShuttlePix P-MFSC, NIKON, Japan). And sequential fluorescent labeled sections were observed under laser scanning confocal microscope (LSCM, A1R MP+, Nikon) using λex/λem of 488/500–550 nm (calcein, green), 543/600–640 nm (alizarin red, red), and 405/560–590 nm (tetracycline hydrochloride, yellow), to assess the time course of bone formation. The amount of the bone-implant contact (BIC) and bone-implant volume (BIV) of the bone inside screw cavity were measured by ImageJ 1.52i (National Institute of Health, USA) as illustrated in Fig. S1C.

2.8. Statistics

All the results are expressed as mean ± standard deviation (SD). Statistical comparisons between groups were analyzed using one-way ANOVA by OriginPro 2020 (OriginLab Co., USA). A value of $p < 0.05$ was considered statistically significant.

3. Results

3.1. The mTi implant and its local static magnetic field

The assembly structure and the static magnetic field (SMF) intensity distribution of the fabricated mTi implant are shown in Fig. 1. The small rod-shaped NdFeB permanent magnet is placed in the internal extension channel of the titanium implant and then closed with a titanium sealing screw (Fig. 1A). The data from Gaussmeter measurements indicate that the interior small magnet with 20 mT magnetic intensity can generate a moderate SMF surrounding the Ti implant, i.e., a magnetic field intensity of 0.3–9.4 mT in the middle position, or 0.2–1.4 mT in the upper or lower position within 5 mm adjacent to the implant (Fig. 1B). The results indicate that the mTi implant can provide a constant and moderate local SMF and offers feasibility for subsequent *in vivo* animal experiments.

3.2. The characteristics of HYH-Fe particles

Fig. 2 shows the morphology, crystal structure, composition, and VSM magnetization curve of the HYH-Fe particles compared with the pure HA particles. The prepared HYH-Fe and HA particles are composed of small melted particles of ~100 nm dimension (Fig. 2A and Fig. S2), which is caused by the 700 °C activation to induce its upconversion fluorescence [7,27]. Both the diffraction spot rings of the (002) and (211) crystal planes in the inset SAED pattern in Fig. 2A, and the characteristic peaks at 25.9° and 32° etc. in the XRD pattern in Fig. 2B clearly exhibit an HA crystal structure (HA: ICDD 09–0432), which is important for preserving the particle bone-bonding bioactivity. The IR and XPS spectra in Fig. 2C and D demonstrate, respectively, the presence of PO_4^{3-}

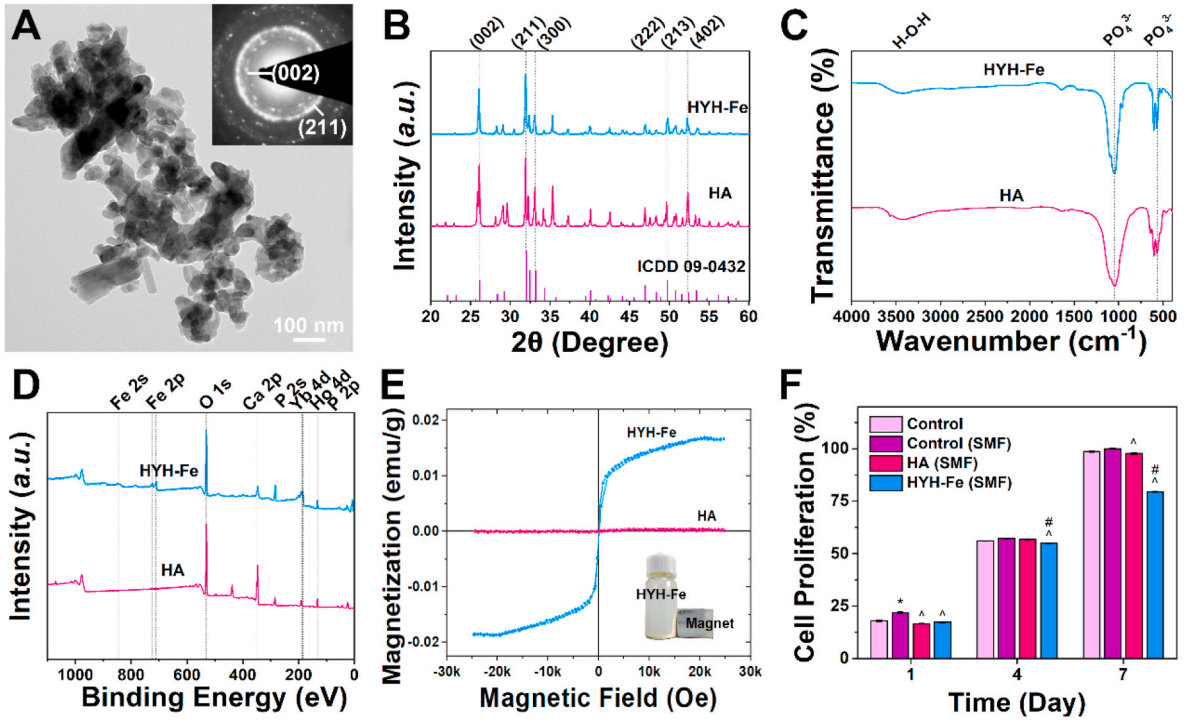

Fig. 2. Synthesis and characterization of the HYH-Fe particles. The TEM morphology and SAED pattern (A) of HYH-Fe particles, the XRD patterns (B), FT-IR spectra (C), XPS spectra (D), VSM magnetization curve and inset magnetic attraction image (E), and *in vitro* cell proliferation (F) of the HYH-Fe compared to pure HA, * vs. Control, ^ vs. Control (SMF), # vs. HA (SMF), for $p < 0.05$.

groups, and Ca, P, O, Yb, Ho, and Fe elements in the HYH-Fe particles. The VSM magnetization curves in Fig. 2E indicate that the HYH-Fe particles possess a superparamagnetic nature while pure HA does not, which is represented by its S-shaped hysteresis loop crossing zero coordinates and the magnetic attraction (inset in Fig. 2E). The measured saturated magnetization (Ms), remanence (Br) and coercivity (Hci) are 19.870×10^{-3} emu/g, 0.637 Oe, and 71.001 Oe, respectively. A special two-step process was used in the preparation of the HYH-Fe particles, i.e., the Yb and Ho ions were firstly doped into the HA crystals and heat treated at 700 °C, then the Fe ions were incorporated on the particle surface region through solution ion exchange, which successfully endow the HYH-Fe particles with both the up-conversion fluorescence (Fig. S3) and the superparamagnetism, and effectively avoid the quenching of the rare earth fluorescence by iron ions.

Fig. 2F shows the cell proliferation with the HYH-Fe and HA particles in the presence of SMF in comparison with the blank control. It shows that the osteoblastic MG63 cells can steadily proliferate with the culture time from day 1 to day 7 for all groups. The SMF does promote the cell proliferation of the control group on day 1 ($p < 0.05$) but is not obvious for the later stage. Overall, the continuous increasing trend of the cell proliferation demonstrates a good cytocompatibility of the HYH-Fe particles although it is relatively weaker than the HA and control. The preparation of the HYH-Fe particles is helpful to study the promotion effect of SMF and superparamagnetic material on early osteogenesis and is also conducive to provide an effective *in vivo* material tracking.

3.3. Micro-CT reconstruction

The micro-CT reconstructed images of the harvested *in vivo* samples were collected through layer-by-layer scanning and image overlapping. Fig. 3A shows the implantation sites of Ti + HA, mTi + HYH-Fe and mTi + HA groups in the mandible of the beagles. All the implants in the three groups are well situated in the mandible bone, and there is no detachment or loosening occurring (Fig. 3B). The single-layer scanning images in Fig. 3C further exhibit the details of the implants, including the sealing screw, internal channel, built-in magnet, and the interface with the surrounding bone tissue. Some small gaps exist between the implant and bone for the Ti + HA and mTi + HA groups; however, the mTi + HYH-Fe group shows closer interface contact without any obvious interface gap (Fig. 3C). It is of note that the bone tissue seems to grow better around the implant in the mTi + HYH-Fe group, i.e., a combination of the SMF and the superparamagnetic HYH-Fe particles may have a promoting effect on the new bone reconstruction.

Fig. 4 and Table 1 show respectively the micro-CT reconstructed bone tissue around the Ti or mTi implants and the corresponding bone volume fraction (BV/TV) and bone trabecula (Tb) after implantation in beagle mandibles for 8 and 12 weeks. The images show that new bone tissue has formed around the threaded surface of the implants in all three groups at 8 weeks, and further thickened at 12 weeks. Table 1 shows that the mTi + HYH-Fe group has the highest BV/TV value and trabecular number (Tb. N) and the smallest trabecular separation (Tb. Sp) at both 8 weeks and 12 weeks, while the trabecular thickness of all groups shows a slight fluctuation. The results indicate that the new bone tissue is growing faster and better in the mTi + HYH-Fe group than the Ti + HA and mTi + HA groups. In addition, the mTi + HA group has a higher BV/TV value than the Ti + HA group, which also means the SMF itself has a certain positive effect on new bone formation.

3.4. Histological analysis

Fig. 5 shows the stained images of histological sections of the samples harvested at 8 and 12 weeks after implantation. At 8 weeks, all three groups display that some trabecular new bone tissue (red) has formed around the Ti implants and should still be growing. There is more trabecular bone around the Ti implant in the mTi + HYH-Fe group than the mTi + HA and Ti + HA groups. At 12 weeks, there is a larger area of new bone tissue surrounding the Ti implants and in contact with the implant surface, particularly for the mTi + HYH-Fe group, which displays more bone tissue around its Ti implant. This result is consistent with the micro-CT images in Figs. 3C and 4 (Table 1). The

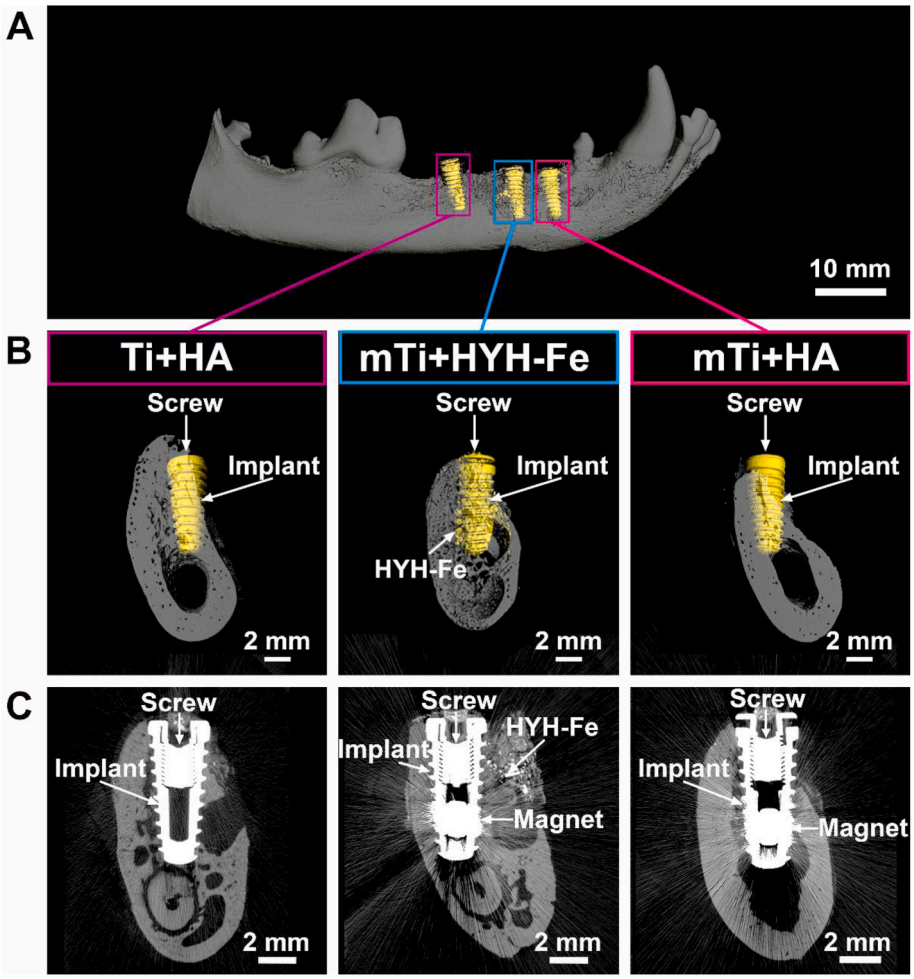

Fig. 3. The micro-CT reconstructed images of Ti + HA, mTi + HYH-Fe and mTi + HA groups. The overall implantation sites (A), the magnified images (B), and the single layer scanning images (C) of the harvested samples after implantation in beagle mandibles for 12 weeks.

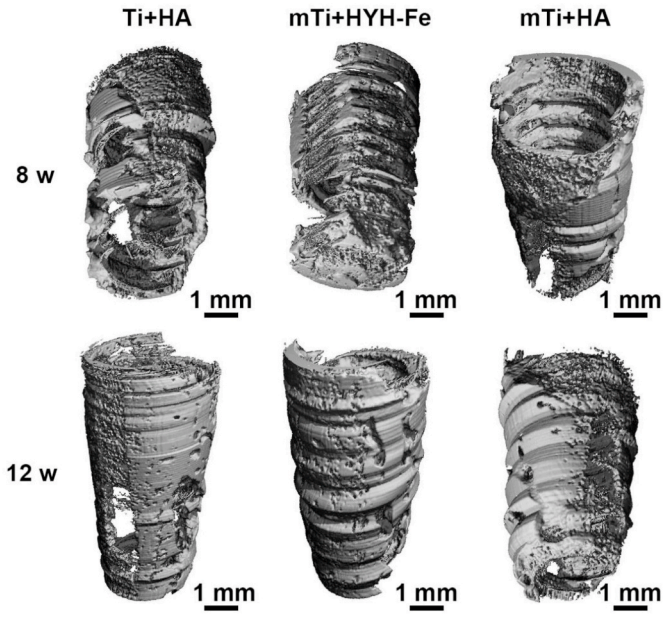

Fig. 4. The micro-CT reconstructed bone tissue around the Ti or mTi implants after implantation in beagle mandibles for 8 and 12 weeks.

Table 1
Bone volume fraction (BV/TV), trabecular number (Tb. N), trabecular thickness (Tb. Th) and trabecular separation (Tb. Sp).

Samples		BV/TV (%)	Tb. N (1/mm)	Tb. Th (mm)	Tb. Sp (mm)
8 w	Ti + HA	27.02	2.52	0.14	0.50
	mTi + HA	29.94	2.86	0.14	0.43
	mTi + HYH-Fe	30.18	3.27	0.16	0.36
12 w	Ti + HA	31.08	3.42	0.12	0.35
	mTi + HA	34.75	3.61	0.16	0.34
	mTi + HYH-Fe	37.53	4.81	0.15	0.23

histomorphometric evaluation of the bone-implant contact (BIC) and bone-implant volume (BIV) is summarized in Table S1 and Fig. 5B–C. The contact area of bone to implant shows a trend of mTi + HYH-Fe > mTi + HA > Ti + HA at both 8 and 12 weeks, demonstrating that SMF or in particular the combination of SMF and superparamagnetic HYH-Fe particles has a positive effect on the promotion of early osteogenesis. Furthermore, the differences in different stages of osteogenesis between the three groups were also revealed by us via the in situ sequential fluorescent labeling of new bone formation.

3.5. The sequential fluorescent labeling of new bone tissue

Fig. 6 exhibits the images of the in situ sequential fluorescence

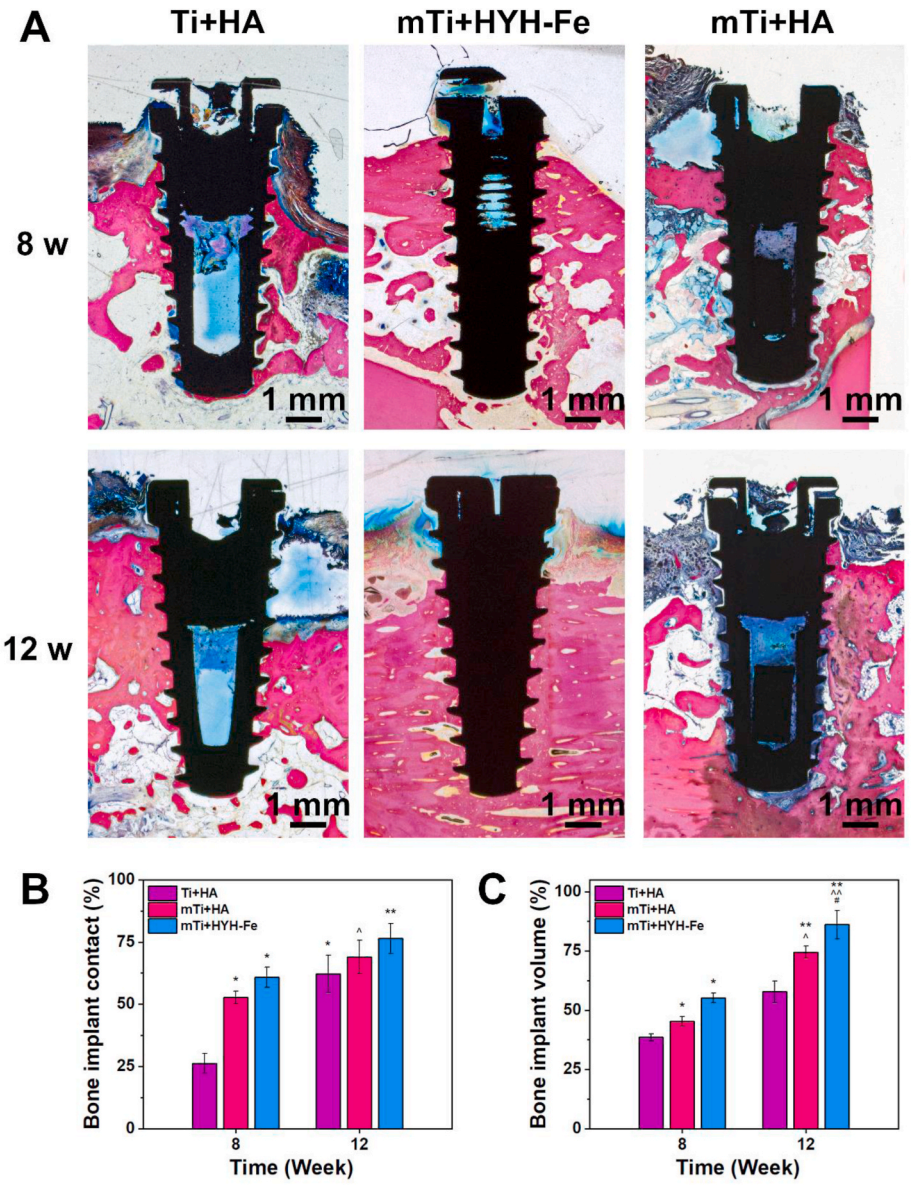

Fig. 5. The histological sections and the histomorphometric evaluation. The stained histological sections of the Ti + HA, mTi + HYH-Fe and mTi + HA groups after implantation in beagle mandibles for 8 and 12 weeks (A). The bone-implant contact (BIC) and bone-implant volume (BIV) of the stained histological sections (B–C). * vs. Ti + HA (8 w), ^ vs. mTi + HA (8 w), # vs. mTi + HYH-Fe (8 w), ** vs. Ti + HA (12 w), ^^ vs. mTi + HA (12 w), for $p < 0.05$.

labeled bone tissue for the three Ti + HA, mTi + HA, and mTi + HYH-Fe groups via LSCM observation. The green, red, and yellow fluorescence represents respectively the new bone tissue formed at 8 weeks labeled by calcein, at 10 weeks labeled by alizarin red, and at 12 weeks labeled by tetracycline. The images show that there has been some new bone tissue (green fluorescence) formed around the Ti implants in all three groups at 8 weeks (Fig. 6A, E, I). At 10 weeks, more new bone tissue (red fluorescence) was further formed around the Ti implants, and even grew into the screw spacing of the implant surface (Fig. 6B, F, J). At 12 weeks, the yellow fluorescent image region of new bone tissue basically corresponds to the red image of 10 weeks (Fig. 6C, G, K), except for a small amount of bone tissue that continues to grow (white arrows in Fig. 6K). The overlay images in Fig. 6D, H, L indicate that the bone tissue formed early (green fluorescence) at 8 weeks does not closely contact with the implant surface, and close contact of new bone with the implant surface nearly starts from 10 weeks. The statistical analysis results of the BIC and BIV from the sequential fluorescent labeled LSCM images of three groups are listed in Table S2 and shown in Fig. 6M – N, which is similar to the histomorphometric evaluation in Fig. 5B–C. It is of note that the BIC at 10 weeks (red regions) are already close to that at 12 weeks (yellow regions) for all groups, which also shows a trend of mTi + HYH-Fe > mTi + HA > Ti + HA at 8, 10 and 12 weeks. The mTi + HA group and in particular the mTi + HYH-Fe group show good osseointegration at 10 weeks, and there is more new bone tissue filled with the thread space of the implants. In other words, week 10 should be selected as a time point to evaluate the effect on early osteogenesis of the three groups. These results demonstrate that a period of 8–12 weeks (2–3 months) is effective for investigating early osteogenesis, and a combination of mTi implant (local SMF) and superparamagnetic HYH-Fe particles has a positive promotion effect on both early osteogenesis and later stage osseointegration.

3.6. *The tracking of HYH-Fe particles*

Compared to pure HA particles, the prepared HYH-Fe particles not only possess good superparamagnetism and distinct micro-CT imaging performance, but also have good up-conversion fluorescence imaging capacity. Under excitation of a 980 nm near-infrared light, the HYH-Fe

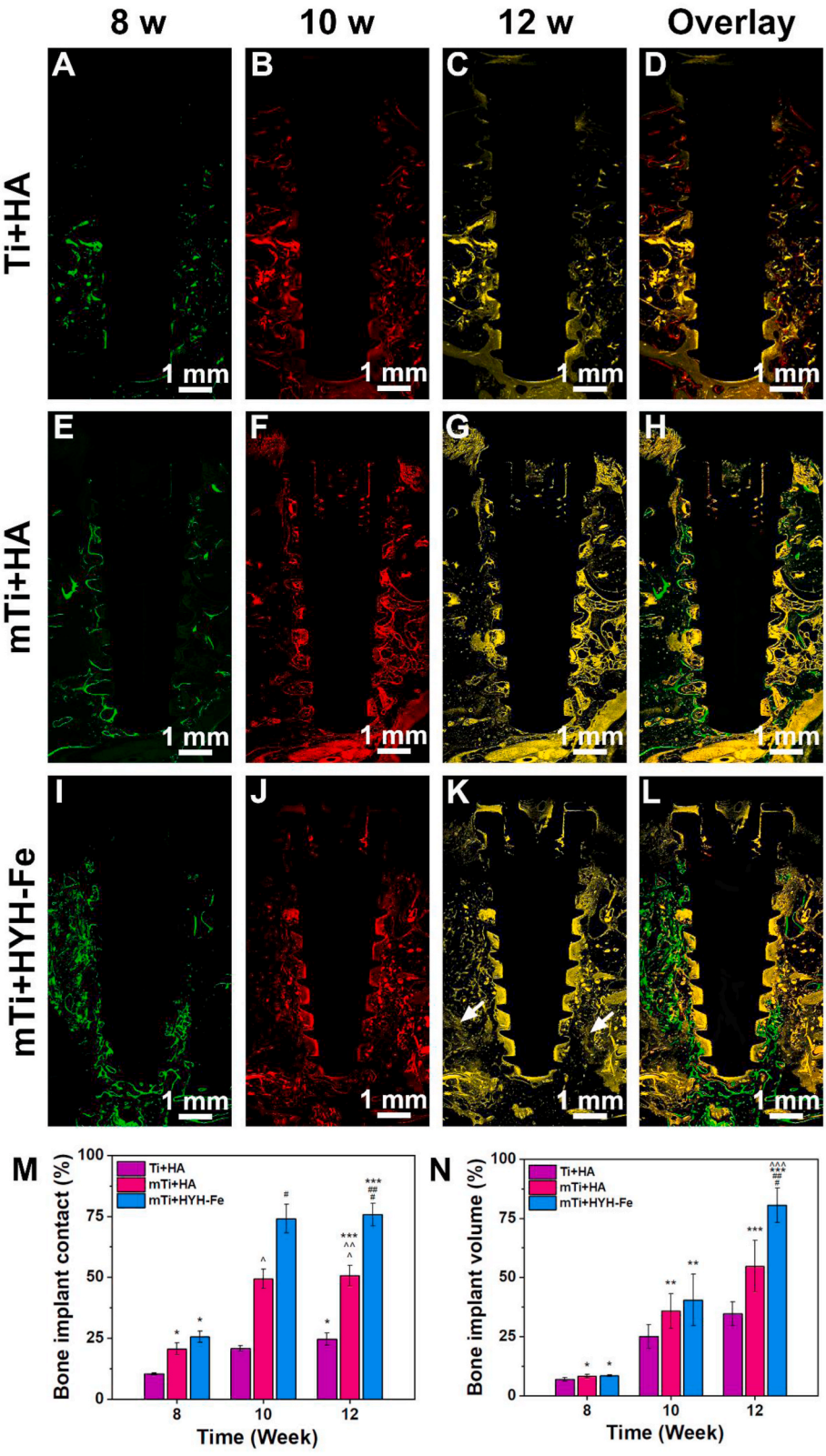

Fig. 6. The LSCM images of the in situ sequential fluorescent labeled bone tissue. The Ti + HA group (A–D), mTi + HA group (E–H) and the mTi + HYH-Fe group (I–L) (Green - bone tissue labeled by calcein at 8 weeks, red - bone tissue labeled by alizarin red at 10 weeks, and yellow - bone tissue labeled by tetracycline at 12 weeks). And the bone-implant contact (BIC) and bone-implant volume (BIV) of the LSCM images (M − N), * vs. Ti + HA (8 w), ^ vs. mTi + HA (8 w), # vs. mTi + HYH-Fe (8 w), ** vs. Ti + HA (10 w), ^^ vs. mTi + HA (10 w), ## vs. mTi + HYH-Fe (10 w), *** vs. Ti + HA (12 w), ^^^ vs. mTi + HA (12 w), for $p < 0.05$. (For interpretation of the references to color in this figure legend, the reader is referred to the Web version of this article.)

particles can emit green fluorescence of 543 nm wavelength due to the co-doping of Yb and Ho ions, while the HA particles have no such characteristic [27]. This enables us to further trace the HYH-Fe particles around the dental implant or in the new bone tissue. As shown in Fig. 7, when overlaying the up-conversion green image of HYH-Fe particles (Fig. 7B) on the tetracycline labeled bone tissue (Fig. 7A), we can clearly observe the implanted HYH-Fe particles remaining in the bone tissue at 12 weeks after implantation (Fig. 7C). As shown by the green fluorescence of the HYH-Fe particles in Fig. 7B, a few agglomerated HYH-Fe particles can be observed at the upper part of the Ti implant, however most of the residual HYH-Fe particles are present in fine particles at 12 weeks, and these fine particles are distributed discretely around the

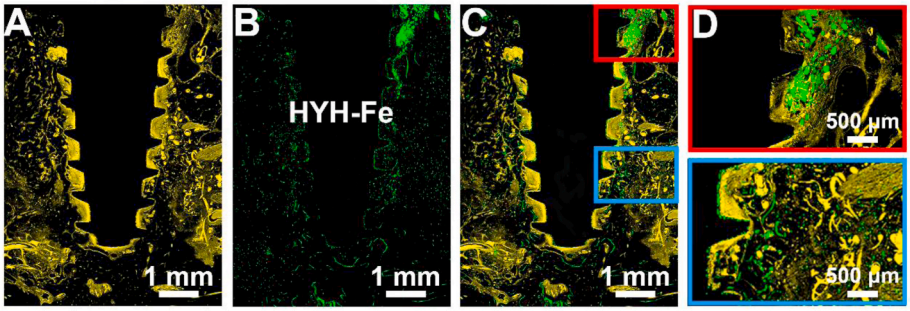

Fig. 7. The tracking of HYH-Fe particles around the implant. The tetracycline labeled bone tissue (A), the green fluorescent image of HYH-Fe particles (B), their overlapping images (C), and the partial enlarged detail (D). (For interpretation of the references to color in this figure legend, the reader is referred to the Web version of this article.)

implant. The enlarged images in Fig. 7D further display that the HYH-Fe particles have integrated with the new bone tissue.

4. Discussion

The purpose of a biomaterial research is to serve in clinical applications to provide advanced materials, new methods, and techniques, while the selection of an animal model is a key aspect in the evaluation of implant materials. Although static magnetic fields (SMF) have no need for external equipment compared to alternating magnetic field, most experimental animal models involving SMF in the past have mainly chosen the femur or femoral condyles of rabbits [7,17], and they are rarely performed directly in the oral environment of large animals. In this study, a small magnetic rod was placed in the extended internal channel of the Ti implant (Fig. 1A), effectively avoiding the cumbersome use of fixed magnets outside the mouth, and making it possible to directly use the Ti implant with its built-in magnet in the mouth of large animals (beagles), and making the results more similar to the human oral environment. This innovative structural design can also avoid direct contact of the magnet with the surrounding tissues without affecting the biocompatibility of the implant.

In this study, the mTi implant shows 0.2–9.4 mT SMF around the Ti implant (Fig. 1B) and can attract the superparamagnetic HYH-Fe particles (inset in Fig. 2E). Such medium strength SMF has been found conducive to cell osteogenic differentiation [29] and to new bone reconstruction [7,30]. The micro-CT scanning images in Fig. 3C shows a closer interface contact for the mTi + HYH-Fe group, while some small gaps exist between the implant and bone for the Ti + HA and mTi + HA groups. The micro-CT reconstructed bone tissue around the Ti implants in Fig. 4 or the corresponding BV/TV values in Table 1, and the stained histological images and BIC/BIV figures in Fig. 5 further indicate that the new bone tissue grew faster and better around the Ti implant in the mTi + HYH-Fe group. All these results demonstrate that the combination of local SMF (mTi) and superparamagnetic HYH-Fe particles has a positive effect on the promotion of early osteogenesis. The pro-osteogenic effect or mechanism should mainly ascribe to two aspects; one might be due to the upregulation of some genes in response to SMF revealed by Kim et al., and the MAPK, Wnt, and PPAR-gamma signaling pathways were closely involved in implant healing [30]. The other should be derived from the magnetic attraction that exert weak but sustained stress on the growing bone tissue [7]. The attraction force of magnetic field on magnetic materials has been found able to in turn exert force on biological tissues, and the stress stimulus can effectively promote bone tissue formation [31,32].

The use of the new superparamagnetic HYH-Fe particles, on the one hand, is beneficial to the study of its effect with the SMF on the promotion of osteogenesis, and on the other hand, it also helps us to track its spatial distribution in the new bone tissue during bone reconstruction. The co-doping of Yb and Ho rare earth ions enables conventional HA material with an up-conversion fluorescence under near-infrared excitation, and can effectively avoid the interference of tissue autofluorescence in the confocal images [27]. Meanwhile, the high X-ray absorbability of the Yb ions [33] will also provide good CT imaging properties for the HA materials. Iron ions usually cause defect traps to interfere with electron transitions and fluorescence emission of the rare earth ions [31,34]; however, in this study, the Fe ions were incorporated only on the surface region of the sintered and solidified HYH particles by ion exchange, effectively avoiding the quenching of Fe ions to the up-conversion fluorescence of the HYH material, although the Fe ions had a weakening effect on the fluorescence (see Fig. S3). This gives the HYH-Fe material good superparamagnetism, upconversion fluorescence and CT (X-ray) imaging properties simultaneously. The upconversion fluorescence and CT imaging capacity of the HYH-Fe material do show superiority in its *in vivo* tracking. As shown in Fig. 7, without the fluorescence given by the HYH-Fe particles, it is difficult to identify and trace the presence and distribution of these particles in the implantation site or in the bone tissue. This multimodal tracking HA material may play an important role in future bone and tooth repair and in long-term postoperative evaluations of the repair effect.

The in situ sequential fluorescent labeling has been demonstrated effective to investigate the new bone formation process at different implantation stages [24–26]. In this study, we employed in situ sequential fluorescent labeling to reveal the differences of early osteogenesis among three groups, including Ti + HA, mTi + HA and mTi + HYH-Fe groups. Compared to the Ti + HA and mTi + HA groups in Fig. 6, the mTi + HYH-Fe group displays faster early osteogenesis and better osseointegration, i.e., a wider range of in situ labeled green fluorescence at 8 weeks (Fig. 6I vs. Fig. 6A, E) and more bone formation in the screw spacing of Ti implant surface at 10 (Fig. 6J) and 12 weeks (Fig. 6K). The images in Fig. 6 also show that the in situ labeled red regions at 10 weeks are already similar to the in situ labeled yellow regions at 12 weeks, and this reminds us that a time point of 10 weeks can be adopted as the identification or evaluation time for the early osteogenesis of the three implantation groups.

5. Conclusions

In general, this research demonstrated the effectiveness of the novel mTi implant combined with the superparamagnetic HYH-Fe particles in promotion of osteogenesis and in tracking of the bone-material interrelations. The mTi implant design not only maintained the titanium implant function but also provided a local static magnetic field, while the HYH-Fe particles exhibited both superparamagnetism and upconversion fluorescence tracking capabilities. The sequential fluorescence labeling results also suggested that week 10 could be adopted as a time point to evaluate the early osteogenesis of the three Ti + HA, mTi + HA, and mTi + HYH-Fe implantation system. The preliminary study paves a new way for investigation on the early osteogenesis of dental implants.

CRediT authorship contribution statement

Xiyu Li: Conceptualization, Methodology, Investigation, Writing - original draft, Writing - review & editing, Visualization, Funding acquisition. **Juan Wu:** Formal analysis. **Danxue Li:** Data curation. **Qin Zou:** Supervision. **Yi Man:** Resources. **Ling Zou:** Validation. **Wei Li:** Project administration.

Declaration of competing interest

The authors declare no competing financial interest.

Acknowledgements

The authors acknowledge the support of funds from the National Natural Science Foundation of China (Grant No. 31700828, 32071335), the Research Funding from West China School/Hospital of Stomatology, Sichuan University (Grant No. RCDWJS2020-9, SKLOD202022). Special thanks to Dr. Li Chen for micro-CT analysis.

Appendix A. Supplementary data

Supplementary data to this article can be found online at https://doi.org/10.1016/j.bioactmat.2021.01.038.

References

[1] Y. Li, Y. Xiao, C. Liu, The horizon of materiobiology: a perspective on material-guided cell behaviors and tissue engineering, Chem. Rev. 117 (5) (2017) 4376–4421.
[2] K.L. Christman, Biomaterials for tissue repair, Science 363 (6425) (2019) 340–341.
[3] N. Jiang, Z. Guo, D. Sun, Y. Li, Y. Yang, C. Chen, L. Zhang, S. Zhu, Promoting osseointegration of Ti implants through micro/nanoscaled hierarchical Ti phosphate/Ti oxide hybrid coating, ACS Nano 12 (8) (2018) 7883–7891.
[4] L.L. Hench, An Introduction to Bioceramics, second ed., World Scientific2013.
[5] A. Carradò, F. Perrin-Schmitt, Q.V. Le, M. Giraudel, C. Fischer, G. Koenig, L. Jacomine, L. Behr, A. Chalom, L. Fiette, A. Morlet, G. Pourroy, Nanoporous hydroxyapatite/sodium titanate bilayer on titanium implants for improved osteointegration, Dent. Mater. 33 (3) (2017) 321–332.
[6] H.S. Kim, Y.J. Kim, J.H. Jang, J.W. Park, Surface engineering of nanostructured titanium implants with bioactive ions, J. Dent. Res. 95 (5) (2016) 558–565.
[7] X. Li, Q. Zou, Y. Man, W. Li, Synergistic effects of novel superparamagnetic/upconversion HA material and Ti/magnet implant on biological performance and long-term in vivo tracking, Small 15 (31) (2019), 1901617.
[8] J. Huang, X. Xia, Q. Zou, J. Ma, S. Jin, J. Li, Y. Zuo, Y. Li, The long-term behaviors and differences in bone reconstruction of three polymer-based scaffolds with different degradability, J. Mater. Chem. B 7 (48) (2019) 7690–7703.
[9] T.G. Wilson, R.J. Miller, R. Trushkowsky, M. Dard, Tapered implants in dentistry: revitalizing concepts with technology: a review, Adv. Dent. Res. 28 (1) (2016) 4–9.
[10] M. Dard, Clinical relevance of integrated developmental research for dental implants, Adv. Dent. Res. 28 (1) (2016) 2–3.
[11] X. Li, Q. Zou, H. Chen, W. Li, In vivo changes of nanoapatite crystals during bone reconstruction and the differences with native bone apatite, Sci. Adv. 5 (11) (2019), eaay6484.
[12] A. Ho-Shui-Ling, J. Bolander, L.E. Rustom, A.W. Johnson, F.P. Luyten, C. Picart, Bone regeneration strategies: engineered scaffolds, bioactive molecules and stem cells current stage and future perspectives, Biomaterials 180 (2018) 143–162.
[13] R. Shi, Y. Huang, C. Ma, C. Wu, W. Tian, Current advances for bone regeneration based on tissue engineering strategies, Front. Med. 13 (2) (2019) 160–188.
[14] K. Schmidt-Bleek, B.M. Willie, P. Schwabe, P. Seemann, G.N. Duda, Bmps in bone regeneration: less is more effective, a paradigm-shift, Cytokine Growth Factor Rev. 27 (2016) 141–148.
[15] F. Wei, Y. Zhou, J. Wang, C. Liu, Y. Xiao, The immunomodulatory role of bmp-2 on macrophages to accelerate osteogenesis, Tissue Eng. 24 (7–8) (2018) 584–594.
[16] K. Sadtler, A. Singh, M.T. Wolf, X. Wang, D.M. Pardoll, J.H. Elisseeff, Design, clinical translation and immunological response of biomaterials in regenerative medicine, Nat. Rev. Mater. 1 (7) (2016) 16040.
[17] A. Ortolani, M. Bianchi, M. Mosca, S. Caravelli, M. Fuiano, M. Marcacci, A. Russo, The prospective opportunities offered by magnetic scaffolds for bone tissue engineering: a review, Joints 4 (4) (2016) 228–235.
[18] M. Marędziak, A. Śmieszek, K.A. Tomaszewski, D. Lewandowski, K. Marycz, The effect of low static magnetic field on osteogenic and adipogenic differentiation potential of human adipose stromal/stem cells, J. Magn. Magn Mater. 398 (2016) 235–245.
[19] K. Marycz, K. Kornicka, M. Röcken, Static magnetic field (SMF) as a regulator of stem cell fate - new perspectives in regenerative medicine arising from an underestimated tool, Stem Cell Rev. Rep. 14 (6) (2018) 785–792.
[20] H. Siadat, S.H. Bassir, M. Alikhasi, Y.S. Shayesteh, A. Khojasteh, A. Monzavi, Effect of static magnetic fields on the osseointegration of immediately placed implants: a randomized controlled clinical trial, Implant Dent. 21 (6) (2012) 491–495.
[21] Y. Yamamoto, Y. Ohsaki, T. Goto, A. Nakasima, T. Iijima, Effects of static magnetic fields on bone formation in rat osteoblast cultures, J. Dent. Res. 82 (12) (2003) 962–966.
[22] R. Leesungbok, S.-J. Ahn, S.-W. Lee, G.-H. Park, J.-S. Kang, J.-J. Choi, The effects of a static magnetic field on bone formation around a sandblasted, large-grit, acid-etched–treated titanium implant, J. Oral Implantol. 39 (s1) (2013) 248–255.
[23] J. Zhang, C. Ding, L. Ren, Y. Zhou, P. Shang, The effects of static magnetic fields on bone, Prog. Biophys. Mol. Biol. 114 (3) (2014) 146–152.
[24] M. Lei, X. Qu, H. Liu, Y. Liu, S. Wang, S. Wu, W.E. Bentley, G.F. Payne, C. Liu, Programmable electrofabrication of porous janus films with tunable janus balance for anisotropic cell guidance and tissue regeneration, Adv. Funct. Mater. 29 (18) (2019), 1900065.
[25] S.M.v. Gaalen, M.C. Kruyt, R.E. Geuze, J.D.d. Bruijn, J. Alblas, W.J.A. Dhert, Use of fluorochrome labels in in vivo bone tissue engineering research, Tissue Eng. Part B 16 (2) (2010) 209–217.
[26] X.q. Jiang, S.y. Wang, J. Zhao, X.l. Zhang, Z.y. Zhang, Sequential fluorescent labeling observation of maxillary sinus augmentation by a tissue-engineered bone complex in canine model, Int. J. Oral Sci. 1 (1) (2009) 39–46.
[27] X. Li, H. Chen, Yb^{3+}/Ho^{3+} co-doped apatite upconversion nanoparticles to distinguish implanted material from bone tissue, ACS Appl. Mater. Interfaces 8 (41) (2016) 27458–27464.
[28] X. Li, Q. Zou, L. Chen, W. Li, A ternary doped single matrix material with dual functions of bone repair and multimodal tracking for applications in orthopedics and dentistry, J. Mater. Chem. B 6 (38) (2018) 6047–6056.
[29] E.-C. Kim, R. Leesungbok, S.-W. Lee, H.-W. Lee, S.H. Park, S.-J. Mah, S.-J. Ahn, Effects of moderate intensity static magnetic fields on human bone marrow-derived mesenchymal stem cells, Bioelectromagnetics 36 (4) (2015) 267–276.
[30] E.-C. Kim, R. Leesungbok, S.-W. Lee, J.-Y. Hong, E.-J. Ko, S.-J. Ahn, Effects of static magnetic fields on bone regeneration of implants in the rabbit: micro-CT, histologic, microarray, and real-time pcr analyses, Clin. Oral Implants Res. 28 (4) (2017) 396–405.
[31] O.A. Tertuliano, J.R. Greer, The nanocomposite nature of bone drives its strength and damage resistance, Nat. Mater. 15 (2016) 1195.
[32] A. Russo, M. Bianchi, M. Sartori, A. Parrilli, S. Panseri, A. Ortolani, M. Sandri, M. Boi, D.M. Salter, M.C. Maltarello, G. Giavaresi, M. Fini, V. Dediu, A. Tampieri, M. Marcacci, Magnetic forces and magnetized biomaterials provide dynamic flux information during bone regeneration, J. Mater. Sci. Mater. Med. 27 (3) (2016) 51.
[33] H. Deng, S. Huang, C. Xu, Intensely red-emitting luminescent upconversion nanoparticles for deep-tissue multimodal bioimaging, Talanta 184 (2018) 461–467.
[34] M.-H. Chen, T. Yoshioka, T. Ikoma, N. Hanagata, F.-H. Lin, J. Tanaka, Photoluminescence and doping mechanism of theranostic Eu^{3+}/Fe^{3+} dual-doped hydroxyapatite nanoparticles, Sci. Technol. Adv. Mater. 15 (5) (2014), 055005.